THE ASTROPHYSICAL JOURNAL, 511:739–749, 1999 February 1
© 1999. The American Astronomical Society. All rights reserved. Printed in U.S.A.

STUDY OF BROAD-SCALE ANISOTROPY OF COSMIC-RAY ARRIVAL DIRECTIONS FROM 2×10^{17} TO 10^{20} ELECTRON VOLTS FROM FLY'S EYE DATA

D. J. BIRD[1]
Department of Physics, University of Illinois at Urbana-Champaign, Urbana, IL 61801

AND

H. Y. DAI,[2] B. R. DAWSON,[3] J. W. ELBERT,[4] M. A. HUANG,[5] D. B. KIEDA, S. KO, E. C. LOH, M. LUO,[6] J. D. SMITH, P. SOKOLSKY, P. SOMMERS, AND S. B. THOMAS
Department of Physics, University of Utah, Salt Lake City, UT 84112
Received 1998 June 11; accepted 1998 September 4

ABSTRACT

We report results on the broad-scale anisotropy of arrival directions of cosmic rays in the energy range from 2×10^{17} to 10^{20} eV. The data were taken by the Fly's Eye detector in both monocular and stereo modes of operation. We look for dependence on galactic latitude or supergalactic latitude by fitting the data to a Wdowczyk and Wolfendale plane enhancement function and a north-south gradient functional form. We report a small but statistically significant galactic plane enhancement in the energy range between 2×10^{17} and 3.2×10^{18} eV. The probability that this anisotropy is due to fluctuations of an isotropic distribution is less than 0.06%. The most significant galactic plane enhancement factor $f_E = 0.104 \pm 0.036$ is in the energy range $(0.4–1.0) \times 10^{18}$ eV. No statistically significant evidence for a north-south gradient is found. There is no sign of significant deviation from isotropic background when the data are analyzed in terms of supergalactic latitude distributions.

Subject headings: cosmic rays — Galaxy: general

1. INTRODUCTION

There have been a number of reports (Gillerman & Watson 1993; Stanev et al. 1995) of small anisotropies in the ultra–high-energy cosmic-ray arrival direction distribution with respect to the Galactic or supergalactic plane. Recently, a high statistics search for anisotropy has been reported by the Akeno Giant Air Shower Array collaboration (Hayashida et al. 1998). This group reports a small anisotropy toward the galactic plane at energies near 10^{18} eV. The statistical significance of this evidence is not strong, however, and the various ground array experiments have reported systematic errors due to temperature and pressure variations and detector energy scale estimation, which are quite different from the systematic errors in Fly's Eye type of experiments. It is therefore important, both from the point of view of statistics and of systematics, to have as complete a picture as possible of all the evidence on anisotropy. This paper is the final result on cosmic-ray anisotropy from the original Fly's Eye experiment (Baltrusaitis et al. 1985; Cassiday 1985), which ran from 1981 to 1992. Previous publications (Bird et al. 1993a, 1993c) were based on subsets of this complete data sample.

Observations of cosmic-ray anisotropy, when taken together with studies of the cosmic-ray spectral shape and cosmic-ray composition, can yield very important clues to the nature of the highest energy cosmic rays. At low energies, cosmic-ray trajectories are affected very significantly by the galactic magnetic field. However, calculations using models of the galactic magnetic field have shown that if cosmic rays above 10^{17} eV come from the galactic plane and are largely protonic in composition, we expect to see a galactic plane enhancement (Smith & Clay 1991). This enhancement will become more significant with increasing energy, since the proton rigidity in the magnetic field will increase. A heavy composition dominated by iron nuclei will tend to show much smaller anisotropy at any given energy because of the smaller Larmor radius of the heavy nuclei. Even so, the gyroradius for 2×10^{17} eV iron nuclei is approximately 50 pc, which is roughly equal to the half-thickness of the galactic gas disk. While there are uncertainties about the form and magnitude of the galactic magnetic field, particularly in the halo region of the galaxy, observation of significant anisotropy would impose important constraints both on the nature of the magnetic field and on the cosmic-ray composition. Previously reported Fly's Eye data on spectrum (Bird et al. 1994) and composition (Bird et al. 1993b, 1993d) support a two-component model where a mostly heavy galactic composition is superseded by a mostly light, extragalactic component. The crossover between these two cosmic-ray fluxes appears to be near 3×10^{18} eV. If correct, this model would imply at best a small galactic plane enhancement below 3×10^{18} eV.

If the higher energy cosmic-ray flux is indeed mostly extragalactic, it may have a different anisotropy from the lower energy component. Strong nearby extragalactic sources could lead to strong anisotropies at energies near 10^{20} eV. If extragalactic magnetic fields are not greater than a nanogauss (Kronberg 1994), charged particle astronomy becomes possible at these energies. It has been recently suggested that extragalactic sources may be distributed along the supergalactic plane (Stanev et al. 1995). If so, we might expect an enhancement of cosmic-ray arrival directions toward this plane at high enough energies. Of course, extra-

[1] Present address: Defence Science and Technology Organisation, P.O. Box 1500, Salisbury, S.A. 5108, Australia.
[2] Present address: Rosetta Inpharmatics, 12040 115th Avenue NE, Kirkland, WA 98034.
[3] Present address: Department of Physics and Mathematical Physics, University of Adelaide, Adelaide, South Australia 5005, Australia.
[4] Present address: 1006 Yakima, Tacoma, WA 94803-2504.
[5] Present address: Institute of Physics, Academia Sinica, 11529 Nankong, Taiwan, ROC.
[6] Present address: Biology Division, Dugway Proving Ground, UT 84002.

galactic sources might have a more complex distribution. They may even reflect the pattern of filaments and voids that are seen in deep space galactic surveys (Waxman, Fisher, & Piran 1996). However, if the origin of the highest energy cosmic rays is due to decay of topological defects (Bhattacharjee, Hill, & Schramm 1992; Bhattacharjee & Sigl 1995), then the anisotropy may have no relation to the distribution of visible matter in the universe.

2. THE FLY'S EYE EXPERIMENT

The Fly's Eye experiment consisted of two detectors (F.E. I and F.E. II) located at Dugway Proving Ground (40° north) in Utah. The two detectors were spaced 3.4 km apart. Details of the experimental technique can be found in Baltrusaitis et al. (1985), Cassiday (1985), and Huang (1996). Briefly, ultra–high-energy cosmic rays entering the atmosphere form an extensive air shower (EAS). The ionizing particles in this shower excite nitrogen fluorescence in the atmosphere. Isotropically emitted light from this fluorescence is collected by spherical mirrors and detected by photomultipliers located at the two detector sites. The photomultiplier tube signals can be used to determine the geometry of the EAS (i.e., its distance from the detector and arrival direction) and the energy of the primary particle. F.E. I had a larger aperture than F.E. II, and events seen by it fall into the monocular data set. Events seen simultaneously by F.E. II (which had a more limited aperture) were classified as stereo events. About one-third of the monocular data set was also seen in stereo. Because events seen in stereo have redundant measurements, the typical stereo geometrical and energy resolution is significantly better than that which is purely monocular. In order to have acceptable resolution, monocular data must be subjected to a number of cuts. The present data sample is large enough that there is still statistical power even after the relatively stringent cuts required.

3. DATA SELECTION AND ANGULAR RESOLUTION

All the Fly's Eye data used in this analysis must pass a standard set of minimum data quality cuts. These cuts remove events that have reconstructed parameters outside their natural range. These cuts also remove events that have estimated parameter errors greater than one-half of their natural range, or have relative parameter error ($\Delta P/P$) greater than 10.0 (Huang 1996).

In this study, we maximize the number of events selected without sacrificing angular resolution. The angular error is defined as the space angle between the input shower direction and the reconstructed one. The tighter the data cut used, the fewer events remain. The optimization is to maximize the ratio of the relative decrease of angular error and the relative decrease of the number of events. We are guided by a Monte Carlo simulation using a two-source model of proton showers and iron showers. This model gives results consistent with the Fly's Eye spectrum and composition results previously reported (Bird et al. 1994, 1993b, 1993d). These simulated events then pass the same event reconstruction programs as the real data. The reconstructed value and the input value for different variables are then compared.

The most important factor controlling the angular error of monocular events is the shower track length. An event with longer track length has more degrees of freedom to determine arrival direction, and, therefore, it has less angular error. We find that the optimal track length is $\geq 50°$.

The data are separated into six energy intervals—E1: 0.2–0.4 EeV; E2: 0.4–1.0 EeV; E3: 1.0–3.2 EeV; E4: 3.2–10 EeV; E5: >10.0 EeV; and E6: >32 EeV. According to the two-source model, E1 should correspond to an almost pure iron composition while E5 and E6 consist of almost pure protons. The width of each energy interval is about half a decade, so we choose the relative energy error $\Delta E/E \leq 3.0$.

A bracket of depth at shower maximum, $X_{\max}$, is also required:

$$300 + 80.0 \times \log_{10}(E) < X_{\max}(\mathrm{g\ cm^{-2}}) < 1100 + 80.0 \times \log_{10}(E)\,, \quad (1)$$

where E is the energy in EeV (1 EeV = 10^{18} eV). Events outside this bracket have poorly reconstructed shower profiles and large angular errors. The relative error of $X_{\max}$ is cut at $\delta X_{\max}/X_{\max} \leq 1.0$. We also require showers to have a reconstructed zenith angle $\leq 80°$.

The Fly's Eye detectors operate on moonless nights. A weather code (Huang 1996) was recorded for every hour of observation. We required data to have been taken when less than one-fourth of the sky is cloudy.

Since we do not know the actual arrival direction of real events, we cannot define the angular error as in Monte Carlo simulated data. We use the uncertainty of the reconstructed value, i.e., the uncertainty in zenith angle $d\theta$ and error in azimuth angle $d\phi$. An overall angular uncertainty is defined as

$$\delta = \sqrt{d\theta^2 + (\sin\theta \times d\phi)^2}\,. \quad (2)$$

This value also shows a strong dependence on track length. Statistically, the mean angular uncertainty is related to the angular error (Huang 1996), but it is impossible to predict

TABLE 1

TIGHT CUTS USED IN THIS STUDY

Parameter	Requirement
Track length	$\geq 50°$
Zenith angle	$\leq 80°$
Angular uncertainty δ[a]	$\leq 15°$
Relative error in energy	$\Delta E/E \leq 3.0$
Relative error in $X_{\max}$	$\Delta X_{\max}/X_{\max} \leq 1.0$
$X_{\max}$	$300 + 80 \times \log_{10}$ (Energy [EeV]) $\leq X_{\max}$(g cm^{-2}) $\leq 1100 + 80 \times \log_{10}$ (Energy [EeV])
Weather	No frost, moderate or no scattering, $<\frac{1}{4}$ sky cloudy.

[a] Angular uncertainty $\delta = \sqrt{d\theta^2 + (\sin\theta \times d\phi)^2}$.

TABLE 2

NUMBER OF EVENTS AND MEAN ENERGY OF EVENTS THAT PASS THE TIGHT CUTS

	ENERGY (EeV)	STEREO		MONO	
		Number	$\langle E \rangle$	Number	$\langle E \rangle$
E1.....	0.2–0.4	2709	0.289	5183	0.287
E2.....	0.4–1.0	2402	0.619	4815	0.621
E3.....	1.0–3.2	1141	1.613	2465	1.658
E4.....	3.2–10.0	191	5.912	597	5.357
E5.....	>10.0	33	16.366	169	22.806
E6.....	>32.0	2	41.786	17	78.282
Total.....		6476		13229	

angular error from angular uncertainty δ on an event-by-event basis. Nonetheless, we applied a cut of $\delta < 15^\circ$ to select the events with the lowest average angular uncertainty.

The tight cuts we used in this study are listed in Table 1. The resulting number of events of mono and stereo data are listed in Table 2. Because the stereo data have only two events at energy greater than 32 EeV, this analysis does not apply to this energy bin.

From Monte Carlo studies, the angular resolution is 3°.2 for monocular data and 1°.1 for stereo data at the 50% confidence level. The 50% confidence level angular resolution is the angular radius of a circle that contains 50% of the reconstructed events from a trial point source. At the 90% confidence level, the angular resolution is 9°.6 for monocular data and 3°.2 for stereo data.

For the stereo subsample, we can compare the same event reconstructed by monocular and stereo methods. The space angle between these two directions is also a measure of the possible angular resolution of this subset of data. Figure 1 shows the resulting Poisson-like distribution of angular resolution. At 50% confidence level, the angular resolution

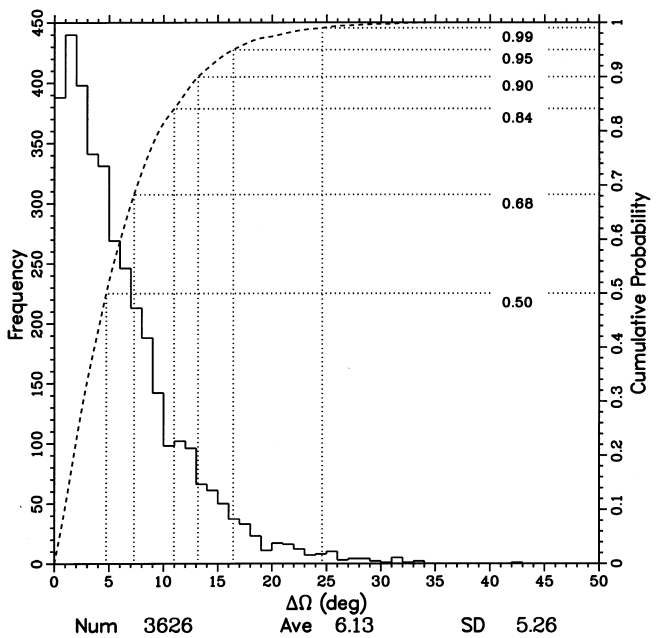

FIG. 1.—Angular resolution of common events in both mono and stereo data. The $\Delta\Omega$ is the space angle between arrival directions reconstructed by monocular and stereo methods.

is approximately 5°.0. In the large-scale anisotropy analysis, in order to have enough statistics in each bin, we choose a bin width of 10° for both monocular and stereo data.

4. ISOTROPIC BACKGROUND PREDICTION

The background expected from an isotropic intensity can, in principle, be calculated by

$$B(l, b, E) = \sum_{\text{operation/nights}} \int_{T_{\text{on}}}^{T_{\text{off}}} R(T) \times A(\theta, \phi, E) dT \ , \quad (3)$$

where $B(l, b, E)$ is the predicted isotropic background at longitude l and latitude b at energy E and $R(T)$ is the event rate at time T. Note that θ and ϕ are here regarded as functions of l, b, and T. $A(\theta, \phi, E)$ is the acceptance of the detector, the geometric efficiency that is the relative ability to detect events of energy E from a certain zenith angle θ and azimuth angle ϕ.

The Fly's Eye event rate $R(T)$ fluctuates because of variations in night sky noise and weather conditions. Instead of attempting to predict $R(T)$ from the weather conditions and using equation (3) to estimate the isotropic background, we use a scrambled event method to derive the background with better accuracy.

From the real data we select the events that pass the weather code cut and store their trigger time in a time data bank. For those events that pass the tight cuts, we store their arrival direction (θ, ϕ) in a direction data bank. The time data bank contains information on the system on/off time and trigger rate $R(T)$. The direction data bank contains the acceptance information. Then a simulated event is generated by randomly sampling a set of (θ, ϕ) from the direction data bank and an event trigger time from the time data bank. This randomization destroys the correlation from any source. The scrambled events thus generate a background data set of isotropic cosmic rays.

On account of improvements in the Fly's Eye detector hardware, the acceptance $A(\theta\phi, E)$ may be different for different hardware epochs. The background is calculated using the time and direction data from the same epoch. However, at energy greater than 3.2 EeV, the number of events is so small that the acceptance becomes indistinguishable between epochs. In order to have proper statistics, we have to combine all epochs to form a direction data bank for this energy range.

In this study, we simulate 5000 sets of data each having the same number of events as real data. The mean value of those 5000 sets is used as the expected detector exposure. The fluctuation of those 5000 sets estimates the uncertainty in this exposure.

5. BROAD-SCALE ANISOTROPY ANALYSIS

We compare the arrival direction distributions for two zones of the sky. The first zone is the whole sky, while the second zone is the half of the sky ($30^\circ < l < 210^\circ$) where the Fly's Eye acceptance covers most of the galactic latitude. We also compare the distribution in supergalactic coordinates.

The null hypothesis of this study is that cosmic rays are isotropically distributed. Based on this hypothesis, we simulate the expected sky distribution and then compare it with the real data distribution. The data and background are binned in 10° latitude bins, and the χ^2 of agreement between

data and background is calculated. We define

$$\chi^2 = \sum_{i=1,\mu} (D_i - B_i)^2 / S_i^2 , \quad (4)$$

where

D_i = number of events in energy E and latitude bin i;
B_i = number of events of isotropic background;
S_i = standard deviation of B_i;
μ = degrees of freedom.

The probability of having a greater or equal χ^2 due to fluctuation in an isotropic distribution is also computed. A large probability shows that the two distributions are similar to each other and therefore consistent with the null hypothesis. Conversely, a small probability shows that the two distributions are incompatible. Table 3 lists the χ^2 and probability $P(>\chi^2, \mu)$.

The error S_i that is the standard deviation of the fluctuation in the isotropic background determined by the scrambled event method does not follow a Poisson distribution exactly. We find that S_i is 93%–95% of $\sqrt{B_i}$, the expected Poisson error. The two can be related by an empirical quadratic form

$$0 = k \times S_i^2 + S_i - \sqrt{B_i} , \quad (5)$$

where k depends on whether we use monocular or stereo data and the sky zones. When B_i is small, S_i approaches $\sqrt{B_i}$.

The probability $P(>\chi^2)$ indicates that some energy intervals may be inconsistent with the isotropic expectation. To find a functional form of this anisotropy, we fit the data to two widely used parameterizations. While these simple forms probably do not represent the actual anisotropy, they allow us to look for broad trends and compare our results with those of other groups in a straightforward manner. A north-south anisotropy in the latitude b_i (GRAD fit)

$$R(b_i) = 1 + f \times b_i \quad (6)$$

could result from nearby extragalactic sources (from the Virgo supercluster, for example). Wdowczyk & Wolfendale (1984; Chi et al. 1993) have proposed that a cosmic-ray excess from the galactic plane can be parameterized in the following form (WWFE fit):

$$R(b_i) = 1 - f + f \times c \times e^{-b_i^2} , \quad (7)$$

where $c = 1.437$ is a normalization constant and f is an energy-dependent galactic enhancement factor. This form does not allow for a variation in the width of the galactic plane enhancement, but at the present level of sensitivity, such a term would be difficult to detect.

We fit the above hypotheses to the data by minimizing χ^2 defined by

$$\chi^2 = \sum_{i=1,N} \frac{(D_i - A_i)^2}{E_i^2} , \quad (8)$$

where

N = number of available bins (*bins* that have $B_i \neq 0$);
A_i = number of expected events in latitude bin i, $A_i = B_i \times R(b_i)$;
E_i = error of A_i.

In this approach, the predicted isotropic background is weighed by the assumed functional form of the anisotropy. The error E_i in the weighed background is then given by the same functional form described above, where B_i is replaced

TABLE 3

THE χ^2 FOR DATA D_i AND ISOTROPIC BACKGROUND B_i

		MONO				MONO		
ENERGY	NUMBER OF EVENTS	μ	χ^2_μ	$P(>\chi^2, \mu)$	NUMBER OF EVENTS	μ	χ^2_μ	$P(>\chi^2, \mu)$
Galactic Latitude, Full Sky								
E1.....	5183	17	1.105	0.341	2709	17	0.715	0.790
E2.....	4815	17	1.355	0.148	2402	17	1.673	0.040
E3.....	2465	17	1.290	0.187	1141	17	0.830	0.659
E4.....	597	17	0.631	0.870	191	17	0.910	0.561
E5.....	169	17	0.988	0.468	33	16	0.714	0.791
E6.....	17	16	0.923	0.545				
Galactic Latitude, Half Sky								
E1.....	4553	16	1.312	0.179	2289	16	0.738	0.757
E2.....	4092	16	1.430	0.117	2031	16	1.279	0.200
E3.....	2040	16	1.071	0.377	972	16	0.655	0.840
E4.....	470	16	0.761	0.731	152	16	0.820	0.664
E5.....	130	16	0.928	0.535	24	15	0.631	0.862
E6.....	14	15	1.000	0.453				
Supergalactic Latitude								
E1.....	5183	17	0.919	0.551	2709	17	1.780	0.025
E2.....	4815	17	1.567	0.064	2402	17	0.601	0.894
E3.....	2465	17	1.313	0.173	1141	17	0.620	0.879
E4.....	597	17	1.090	0.356	191	17	0.757	0.745
E5.....	169	17	1.278	0.195	33	17	0.915	0.556
E6.....	17	17	0.727	0.778				

by A_i. E_i can thus be calculated by solving

$$k \times E_i^2 + E_i - \sqrt{A_i} = 0 , \tag{9}$$

$$E_i = \frac{-1 + \sqrt{1 + 4k\sqrt{A_i}}}{2k} . \tag{10}$$

Figure 2 shows the difference $S_i - \sqrt{B_i}$. We also show the best fit to the above quadratic form. We use this relation to find the error E_i for any given A_i.

To determine if the data require a particular functional form (GRAD or WWFE), we perform an F-test on the difference of χ^2:

$$F = \frac{\chi_0^2 - \chi_{\min}^2}{\chi_{\min}^2/\mathrm{dof}} \tag{11}$$

where

χ_0^2 = original χ^2 without functional form [$R(b) = 1$];
$\chi_{\min}^2$ = χ^2 of best fit;
dof = degrees of freedom.

The number of dof equals N–1 for the full-sky zone and the supergalactic zone. For the half-sky zone, we remove one more dof to properly normalize the total number of events. The probability of the F-test, prob (F; 1; dof), is then calculated. A small probability suggests that the trial functional form is an appropriate description of the experimental data.

The error of the fit parameter f is calculated by a similar process. The upper and lower bounds on f are the values of f at $\chi_{\min}^2 + 1$. The error df is then calculated as one-half of the difference of the upper and lower bound.

The same procedures are applied to the 5000 simulated data sets. The result of these fits provides a check on the systematic error of the fit procedure. The significance of the fit to the data (f_{data}) should be compared to the mean fitted value (f_{mean}) and standard deviation (f_{sd}) of the fitted value of all simulated data sets. Then σ is defined as

$$\sigma = \frac{f_{\mathrm{data}} - f_{\mathrm{mean}}}{f_{\mathrm{sd}}} \tag{12}$$

A single-side Gaussian probability of this σ is also calculated

$$P_{\mathrm{gauss}} = \frac{1}{\sqrt{2\pi}} \int_{\sigma}^{\infty} e^{-z^2/2}\, dz \tag{13}$$

To compare the data with the simulated data sets, a probability of having a greater fitted value is calculated by

$$P_{\mathrm{sim}}(>f_{\mathrm{data}}) = \frac{\text{number of data sets that generate } f > f_{\mathrm{data}}}{\text{total number of data sets}} \tag{14}$$

The total number of simulated data sets is 5000. Figure 3 shows the histogram of the WWFE fit parameter f_E for the simulated isotropic data sets. The distribution of fit parameters can be fitted to a Gaussian form. This figure shows the statistical fluctuation of an isotropic background. The fit parameter for the real data, f_{data}, is shown by the solid arrow.

A small value of probability ($P < 0.05$) suggests the fit parameter is large compared with the fluctuation of iso-

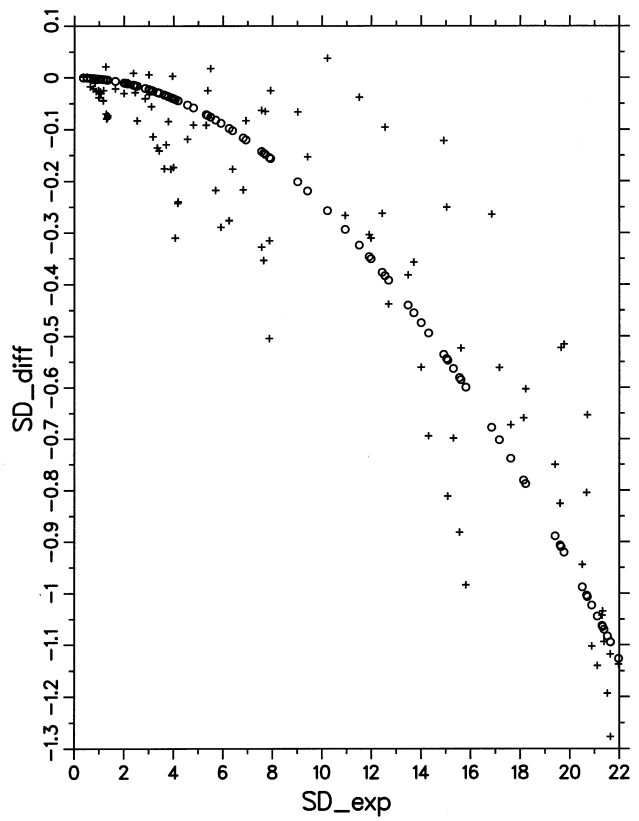

FIG. 2.—X-axis is $\sqrt{B_i}$, the expected error from Poisson distribution. The Y-axis is the difference between the observed scrambled event method standard deviation and the expected Poisson error $S_i - \sqrt{B_i}$, shown as crosses, and the fitted error difference $E_i - \sqrt{B_i}$, shown as circles.

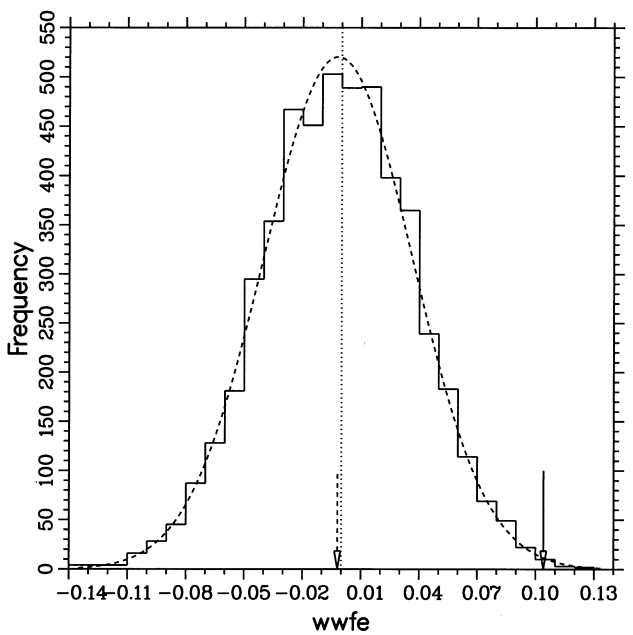

FIG. 3.—Histogram of the WWFE fit parameter for monocular data using the full sky at energy of 0.4–1.0 EeV. The probability P_{sim} is the histogram area from the fit parameter for the data (f_{data}, *solid arrow*) to the right end of axis. Similarly, the P_{gauss} is the area of the fitted Gaussian form from the fit to the right end of the axis. The mean is 0.0020, the WWFE is 0.1040, the standard deviation is 0.0383, and the probability is 0.0022.

TABLE 4

RESULTS FOR WWFE FITTING USING THE FULL-SKY DATA

E	Data	f	df	$\chi^2_{\min}$	F	$P(F)$[a]	f_{mean}	f_{SD}	P_{gauss}	P_{sim}
E1.....	Mono	0.067	0.035	0.943	3.922	0.065	−0.003	0.037	0.030	0.029
	Stereo	0.016	0.047	0.753	0.151	0.702	−0.003	0.050	0.352	0.354
E2.....	Mono	0.104	0.036	0.955	8.120	0.012	−0.002	0.038	0.003	0.002
	Stereo	0.109	0.052	1.505	2.896	0.108	−0.004	0.054	0.018	0.016
E3.....	Mono	0.063	0.052	1.279	1.145	0.300	−0.004	0.056	0.116	0.116
	Stereo	0.079	0.080	0.823	1.152	0.299	−0.008	0.077	0.128	0.132
E4.....	Mono	−0.072	0.113	0.645	0.635	0.437	−0.016	0.111	0.694	0.705
	Stereo	−0.049	0.183	0.963	0.075	0.787	−0.044	0.195	0.511	0.514
E5.....	Mono	−0.264	0.218	0.954	1.616	0.222	−0.061	0.225	0.817	0.818
	Stereo	−0.576	0.402	0.631	3.235	0.091	−0.232	0.454	0.776	0.774
E6.....	Mono	−1.263	0.447	0.618	9.379	0.007	−0.243	0.580	0.961	0.959

[a] $P(F)$ is the F-test probability, prob (F; 1; dof).

tropic background. A large value ($P > 0.95$) suggests that the fit parameter is small.

Tables 4, 5, 6, and 7 list the fit results in galactic coordinates. Tables 8 and 9 list the fit results in supergalactic coordinates. Figures 4, 5, 6, 7, 8, and 9 show the fit results for various conditions.

6. DISCUSSION

6.1. *Systematic Errors*

Because of the limited coverage of galactic latitude, the isotropic background does not always produce a null plane enhancement factor or gradient. However, the systematic bias is negligible for energies less than 3.2 EeV. The systematic bias is higher for energy greater than 3.2 EeV; for these energies the fit parameter may not represent the true magnitude of the anisotropy. However, the significance and probability are not affected by this bias, because the actual data are compared with simulated data sets according to equation (14). The probabilities quoted in the latter part of this article all come from P_{sim}.

We also make a study of the systematic bias by reducing the number of events in each energy bin and redoing the fitting. Figure 10 shows the distribution of fit parameters and background as a function of total number of events. This study shows that the fit result does not depend strong-

TABLE 5

RESULTS FOR WWFE FITTING USING THE HALF-SKY DATA

E	Data	f	df	$\chi^2_{\min}$	F	$P(F)$[a]	f_{mean}	f_{SD}	P_{gauss}	P_{sim}
E1.....	Mono	0.096	0.040	1.016	5.659	0.031	−0.003	0.042	0.009	0.008
	Stereo	0.045	0.056	0.745	0.864	0.367	−0.006	0.058	0.194	0.196
E2.....	Mono	0.126	0.043	0.972	8.539	0.011	−0.003	0.045	0.002	0.002
	Stereo	0.113	0.061	1.144	2.879	0.110	−0.006	0.063	0.029	0.031
E3.....	Mono	0.024	0.060	1.132	0.137	0.716	−0.007	0.064	0.318	0.317
	Stereo	−0.039	0.093	0.687	0.252	0.623	−0.014	0.091	0.608	0.615
E4.....	Mono	−0.156	0.130	0.715	2.042	0.173	−0.026	0.131	0.839	0.844
	Stereo	0.098	0.215	0.862	0.233	0.636	−0.073	0.228	0.227	0.226
E5.....	Mono	−0.261	0.252	0.915	1.230	0.285	−0.094	0.261	0.739	0.737
	Stereo	−0.486	0.454	0.596	1.941	0.184	−0.319	0.509	0.629	0.627
E6.....	Mono	−1.448	0.428	0.608	11.313	0.004	−0.323	0.668	0.954	0.959

[a] $P(F)$ is the F-test probability, prob (F; 1; dof).

TABLE 6

RESULTS FOR GRADIENT FITTING USING THE FULL-SKY DATA

E	Data	f	df	$\chi^2_{\min}$	F	$P(F)$[a]	f_{mean}	f_{SD}	P_{gauss}	P_{sim}
E1.....	Mono	−0.050	0.021	0.832	6.569	0.021	−0.001	0.022	0.987	0.985
	Stereo	0.040	0.029	0.638	3.077	0.099	−0.001	0.028	0.074	0.072
E2.....	Mono	−0.021	0.023	1.385	0.628	0.440	−0.001	0.023	0.811	0.803
	Stereo	−0.053	0.030	1.582	1.975	0.179	−0.001	0.031	0.955	0.952
E3.....	Mono	−0.052	0.030	1.188	2.458	0.136	−0.001	0.031	0.947	0.947
	Stereo	−0.098	0.043	0.576	8.507	0.010	−0.002	0.045	0.984	0.986
E4.....	Mono	0.072	0.064	0.589	2.229	0.155	−0.005	0.062	0.107	0.105
	Stereo	0.066	0.105	0.943	0.417	0.528	−0.012	0.104	0.228	0.225
E5.....	Mono	−0.033	0.113	1.045	0.082	0.779	−0.016	0.125	0.555	0.547
	Stereo	0.134	0.204	0.733	0.565	0.463	−0.021	0.245	0.263	0.257
E6.....	Mono	−0.114	0.191	0.961	0.341	0.567	−0.051	0.325	0.576	0.544

[a] $P(F)$ is the F-test probability, prob (F; 1; dof).

TABLE 7

RESULTS FOR GRADIENT FIT USING THE HALF-SKY DATA

E	Data	f	df	$\chi^2_{\rm min}$	F	$P(F)$[a]	$f_{\rm mean}$	$f_{\rm SD}$	$P_{\rm gauss}$	$P_{\rm sim}$
E1.....	Mono	−0.066	0.024	0.897	8.411	0.011	−0.001	0.024	0.997	0.997
	Stereo	0.028	0.034	0.742	0.928	0.351	−0.001	0.033	0.193	0.191
E2.....	Mono	−0.017	0.026	1.497	0.286	0.600	−0.001	0.026	0.738	0.731
	Stereo	−0.050	0.035	1.228	1.662	0.217	−0.001	0.035	0.919	0.920
E3.....	Mono	−0.026	0.034	1.106	0.491	0.494	−0.001	0.036	0.758	0.755
	Stereo	−0.053	0.049	0.622	1.836	0.196	−0.001	0.052	0.841	0.843
E4.....	Mono	0.058	0.069	0.766	0.898	0.358	−0.003	0.072	0.198	0.197
	Stereo	0.027	0.127	0.872	0.054	0.819	−0.002	0.120	0.403	0.398
E5.....	Mono	0.048	0.144	0.983	0.112	0.743	−0.011	0.143	0.339	0.339
	Stereo	−0.058	0.267	0.670	0.071	0.793	0.017	0.281	0.606	0.597
E6.....	Mono	−0.133	0.215	1.042	0.352	0.562	−0.028	0.373	0.611	0.594

[a] $P(F)$ is the F-test probability, prob (F; 1; dof).

ly on event number. However, when the number of events falls below 100, the isotropic background begins to give f_E significantly different from 0. This systematic bias is clearly an artifact of low statistics. We suspect that the large negative f_E reported in some studies (Chi et al. 1993) could also be affected by the large bias inherent in low statistic data samples.

The other systematic effect is a non-Poisson distribution of errors. If we use the square root of the expected number $\sqrt{B_i}$ as the error, we will overestimate the error in higher event count regions, typically galactic latitudes $-25°$ to $65°$. By using the fitted error, we improve both the χ^2-value and the accuracy of the fit.

6.2. *Anisotropy in Galactic Coordinates*

To search for anisotropy, we first look at the χ^2 between data and isotropic background. The $P(>\chi^2, \mu)$ in Table 10 shows that E2 has $P(>\chi^2, \mu)$ less than 0.20 for all data. This may indicate that the data distribution is inconsistent with an isotropic background. On the other hand, for E4, all the $P(>\chi^2, \mu)$ are larger than 0.5. This might suggest that the cosmic-ray distribution at E4 is consistent with an isotropic background.

The most significant result is the WWFE fit for E2 (0.4–1.0 EeV). The significance varies from 0.031 to 0.002. Both mono and stereo data give the fit plane enhancement factor

TABLE 8

RESULTS FOR WWFE FITTING USING THE SUPERGALACTIC LATITUDE

E	Data	f	df	$\chi^2_{\rm min}$	F	$P(F)$[a]	$f_{\rm mean}$	$f_{\rm SD}$	$P_{\rm gauss}$	$P_{\rm sim}$
E1.....	Mono	−0.004	0.038	0.975	0.013	0.910	−0.002	0.039	0.518	0.525
	Stereo	−0.052	0.050	1.824	0.592	0.453	−0.004	0.052	0.824	0.827
E2.....	Mono	−0.095	0.038	1.247	5.368	0.034	−0.002	0.038	0.992	0.991
	Stereo	−0.051	0.052	0.580	1.634	0.219	−0.004	0.054	0.807	0.808
E3.....	Mono	−0.019	0.052	1.387	0.094	0.763	−0.004	0.054	0.611	0.623
	Stereo	−0.066	0.078	0.613	1.204	0.289	−0.008	0.077	0.775	0.770
E4.....	Mono	−0.012	0.108	1.157	0.011	0.916	−0.015	0.108	0.488	0.487
	Stereo	0.113	0.178	0.780	0.495	0.492	−0.039	0.185	0.206	0.204
E5.....	Mono	0.075	0.203	1.350	0.101	0.755	−0.059	0.219	0.271	0.281
	Stereo	−0.124	0.322	0.963	0.157	0.697	−0.206	0.430	0.425	0.439
E6.....	Mono	−0.208	0.456	0.759	0.281	0.603	−0.239	0.569	0.478	0.475

[a] $P(F)$ is the F-test probability, prob (F; 1; dof).

TABLE 9

RESULTS FOR GRADIENT FIT USING THE SUPERGALACTIC LATITUDE

E	Data	f	df	$\chi^2_{\rm min}$	F	$P(F)$[a]	$f_{\rm mean}$	$f_{\rm SD}$	$P_{\rm gauss}$	$P_{\rm sim}$
E1.....	Mono	0.001	0.021	0.976	0.003	0.954	−0.001	0.023	0.471	0.460
	Stereo	−0.001	0.028	1.891	0.001	0.974	−0.001	0.030	0.500	0.489
E2.....	Mono	0.005	0.021	1.661	0.033	0.858	−0.001	0.022	0.398	0.394
	Stereo	0.017	0.030	0.617	0.557	0.466	−0.001	0.031	0.280	0.276
E3.....	Mono	−0.047	0.029	1.235	2.071	0.169	−0.001	0.031	0.928	0.924
	Stereo	0.000	0.043	0.659	0.000	1.000	−0.002	0.044	0.481	0.472
E4.....	Mono	0.010	0.061	1.156	0.024	0.880	−0.004	0.061	0.408	0.400
	Stereo	−0.065	0.103	0.780	0.493	0.493	−0.106	0.102	0.704	0.700
E5.....	Mono	−0.273	0.119	1.048	4.736	0.045	−0.014	0.126	0.981	0.981
	Stereo	0.168	0.265	0.945	0.454	0.510	−0.039	0.237	0.191	0.185
E6.....	Mono	−0.178	0.250	0.742	0.662	0.428	−0.045	0.320	0.661	0.638

[a] $P(F)$ is the F-test probability, prob (F; 1; dof).

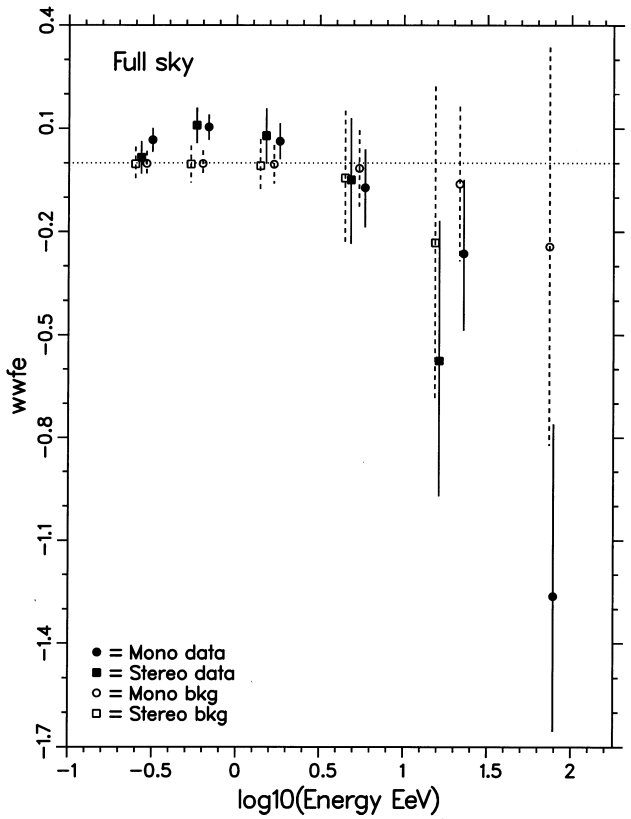

FIG. 4.—WWFE fit using the full-sky data

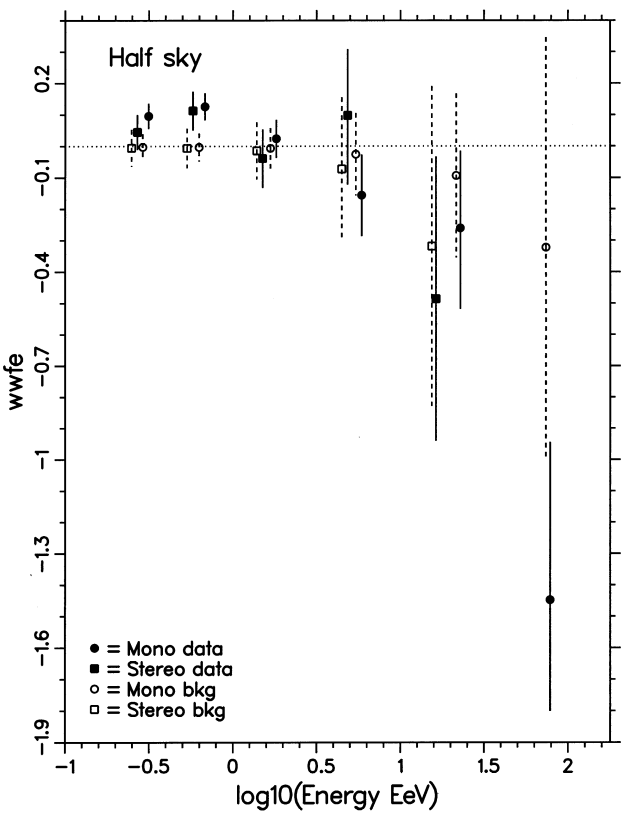

FIG. 5.—WWFE fit using the half-sky data

f_E at about 0.10. The F-test probabilities, 0.012 for mono and 0.108 for stereo, also show that such a WWFE fit indeed reduces the χ^2. A nonzero f_E is needed to fit the data. Finally, the isotropic background has a chance probability $P_{\rm sim} = 0.002$ for mono data and 0.016 for stereo data to produce f_E larger than the f_E of the data. The gradient fit produces $P_{\rm sim} = 0.731$–0.952 or $\sim 2\ \sigma$, which is not sufficiently significant. The data thus support a small anisotropy in E2 (0.4–1.0 EeV). Figure 11 shows the number of events, event rate, and significance in the E2 bin.

Table 10 lists the probability values of all the fits. The table shows that most of the fits have similar probability for full-sky and half-sky zones except the WWFE fit to stereo data at E3. A similar result can be found for mono and stereo data except for the E1 gradient fit and the E4 WWFE fit.

Based on previous F.E. results on spectrum and composition, we expect that the anisotropy in the energy range below 3.0 EeV may be different from that of the higher energy flux. The lower energy data appear to be of a heavier composition and are likely to be of a galactic origin. We can separate data into two groups: group 1 consists of E1–E3 and has energy less than 3.2 EeV; and group 2 consists of E4–E6 and has energy greater than 3.2 EeV. We use compound probability (eqs. [15] and [16]; Fisher 1958; Eadie et al. 1971) to combine probabilities in Table 10. The results are listed in Table 11.

$$p' = P(E1) \times P(E2) \times P(E3)\,, \tag{15}$$

$$\mathrm{CP} = p' \times [1.0 - \log\,(p') + \tfrac{1}{2}\,(\log\,p')^2]\,. \tag{16}$$

Table 11 shows that group 1 supports a positive f_E at approximately 3.2–3.3 σ for monocular data and 1.4–1.9 σ for stereo data. This result suggests that cosmic rays with energy less than 3.2 EeV may have a small anisotropy related to the galactic plane. The stereo data have a less

TABLE 10

THE PROBABILITY $P_{\rm sim}(>f_{\rm data})$ FOR ALL FITS

	WWFE							
	Mono		Stereo		GRAD			
ENERGY	Full	Half	Full	Half	Full	Half	Full	Half
E1.....	0.0292	0.0080	0.3544	0.1962	0.9852	0.9966	0.0722	0.1910
E2.....	0.0022	0.0022	0.0162	0.0312	0.8028	0.7308	0.9524	0.9196
E3.....	0.1162	0.3166	0.1316	0.6148	0.9472	0.7550	0.9860	0.8432
E4.....	0.7048	0.8438	0.5142	0.2258	0.1046	0.1968	0.2254	0.3976
E5.....	0.8178	0.7372	0.7744	0.6266	0.5474	0.3386	0.2574	0.5972
E6.....	0.9590	0.9590	...	...	0.5444	0.5942	...	...

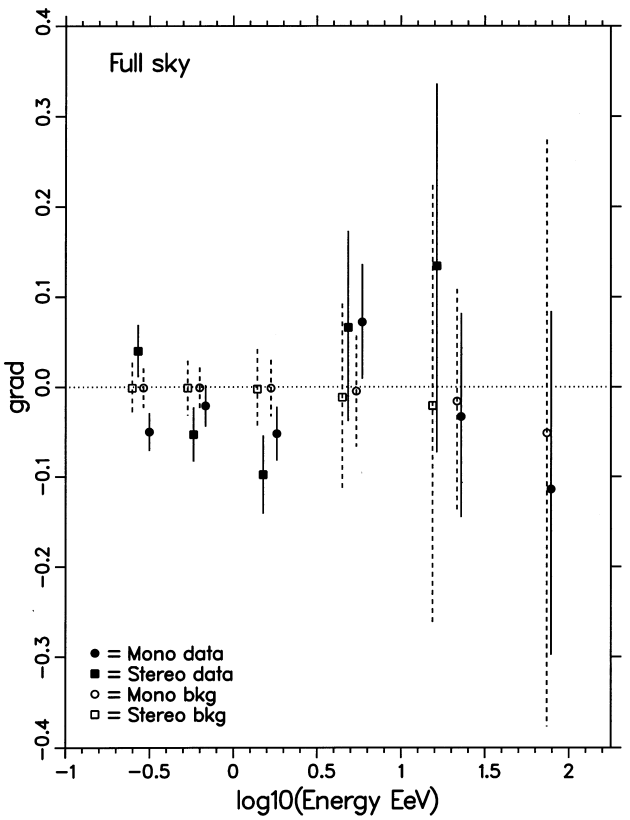

FIG. 6.—Gradient fit using the full-sky data

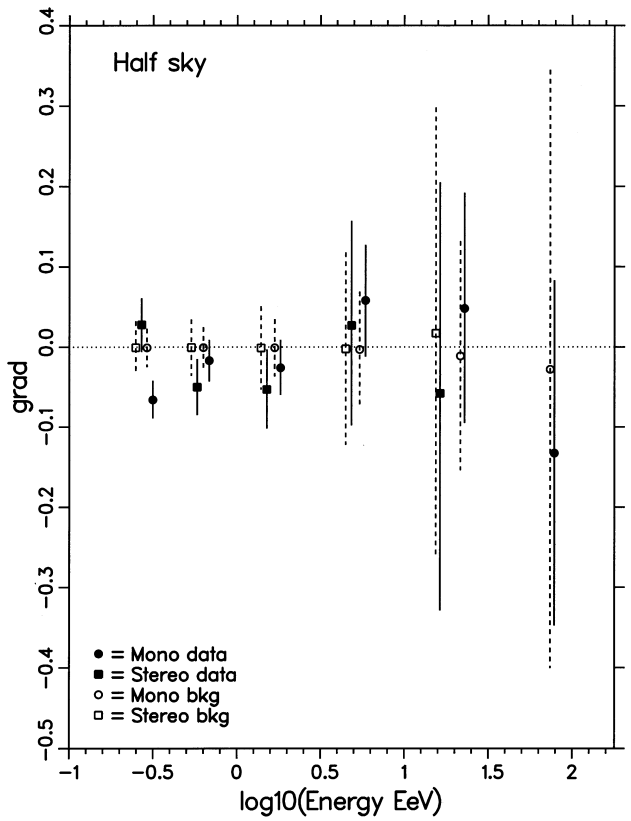

FIG. 7.—Gradient fit using the half-sky data

significant anisotropy because of a very small f_E and large probability at E1 (0.2–0.4 EeV). Detailed comparison between mono data and stereo data shows that there is in fact an excess of events near the galactic center in the mono data. However, the stereo data acceptance is small in this region because of smaller zenith angle coverage. For the galactic latitude gradient, the compound probabilities are in disagreement between monocular data and stereo data.

For group 2, both mono and stereo data have no signs of galactic plane enhancements. The gradient fit shows nothing significant again. Cosmic rays with energy greater than 3.2 EeV are consistent with an isotropic background. Because of the low statistics and large background bias for energy greater than 10 EeV, we cannot support any strong conclusions about anisotropy in this energy region.

6.3. *Anisotropy in Supergalactic Coordinates*

Table 12 lists the probability $P_{\rm sim}$ of mono and stereo data in supergalactic coordinates. Although the E2 f_E fit has a $P_{\rm sim} = 0.9924$ (approximately $-2\ \sigma$), the event distribution shows that the excess of events comes from supergalactic latitude greater than $+70°$ or less than $-70°$, i.e., regions where an excess from the galactic plane could be having a strong effect. This supergalactic polar excess is not significant either in individual bin (E2 mono data 2.38 σ) or over three energy bins (E1–E3). Contrary to the Stanev et al. (1995) result, we do not see evidence of anisotropy coming from the supergalactic plane for energies greater than 10 EeV. However, this result is consistent with (Kewley, Clay, & Dawson (1996). They did not find excess of supergalactic plane in the southern sky either.

TABLE 11

THE COMPOUND PROBABILITY AND SIGMA OF ALL THE FITS

	MONO				STEREO			
	Full		Half		Full		Half	
	CP	σ	CP	σ	CP	σ	CP	σ
Group 1								
WWFE CP.....	0.0006	3.2315	0.0005	3.3016	0.0257	1.9481	0.0834	1.3825
GRAD CP	0.9968	−2.7227	0.9771	−1.9968	0.4958	0.0106	0.7011	−0.5275
Group 2[a]								
WWFE CP.....	0.9776	−2.0063	0.9843	−2.1525	0.7649	−0.7220	0.4182	0.2066
GRAD CP	0.3268	0.4489	0.3739	0.3216	0.2232	0.7615	0.5789	−0.1989

[a] For the stereo data group 2 includes only E4–E5.

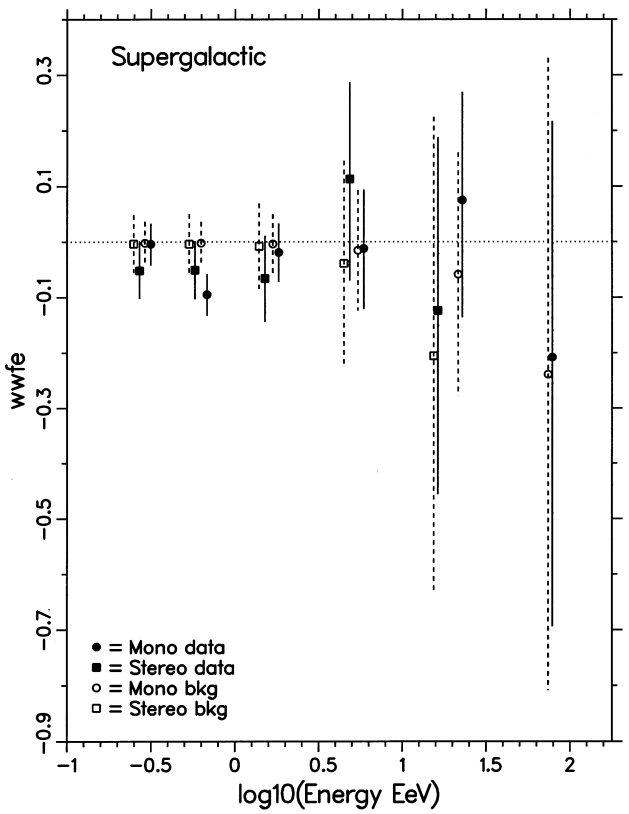

FIG. 8.—WWFE fit using the supergalactic latitude

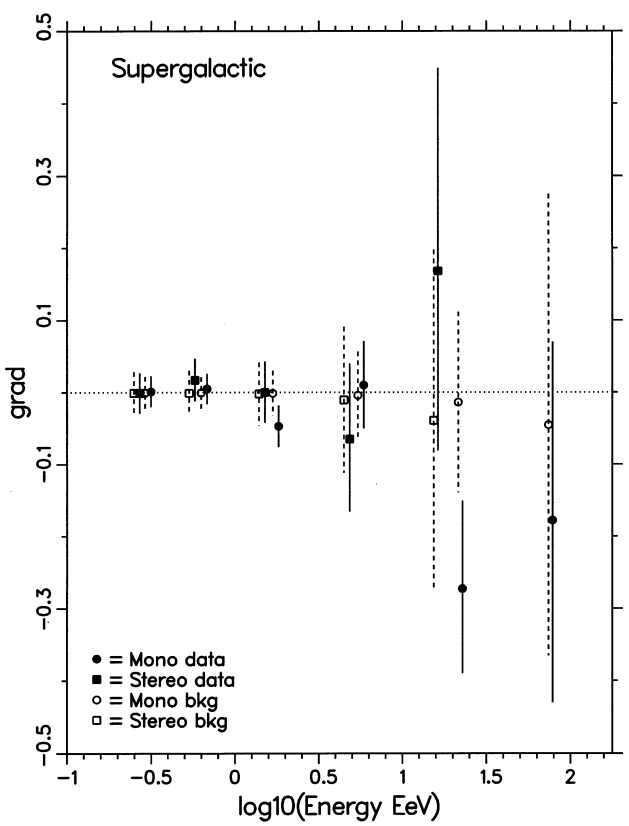

FIG. 9.—Gradient fit using the supergalactic latitude

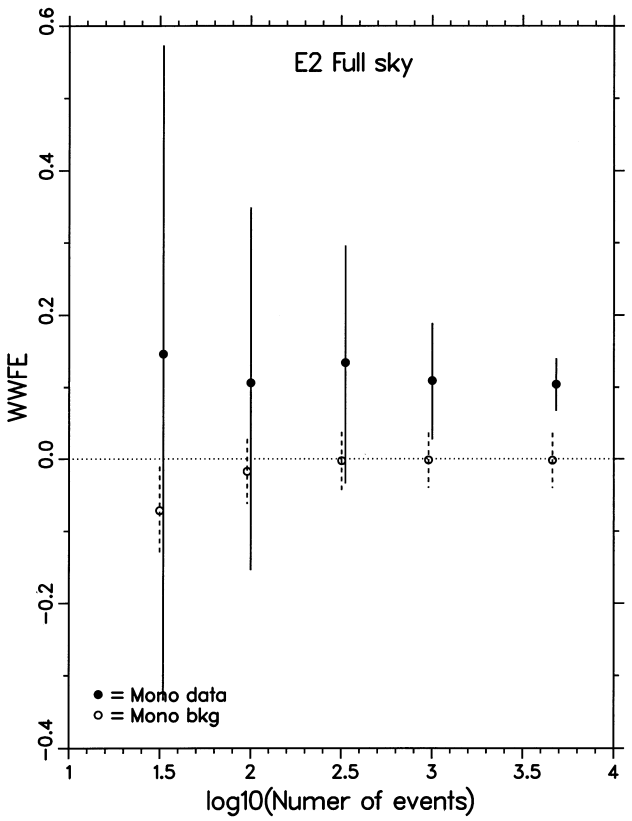

FIG. 10.—WWFE fit of E2 monocular data. The total number of events are reduced from 4815 to 1000, 333, 100, and 33. The solid dots represent the data and mean value of the simulated background are given by circles.

6.4. *Comparison with Other Results*

Most ground array experiments use harmonic analysis to look for anisotropy. However, the Fly's Eye does not have uniform coverage in right ascension, making harmonic analysis difficult to interpret.

There are several reports on the anisotropy toward the galactic plane. Gillerman & Watson (1993) combined several groups of data on f_E and calculated the χ^2 for a null fit ($f_E = 0$). They report a $\chi^2_\mu = 2.2$, or a probability of 0.9%, that f_E is consistent with zero. There may be problems with possible different energy scales between these groups of data. In this study we use the same data set, therefore there is no problem with energy cross calibration. The overall result still supports a modest enhancement from the galactic plane.

TABLE 12

THE PROBABILITY $P_{\rm sim}(>f_{\rm data})$ FOR ALL THE FITS IN SUPERGALACTIC LATITUDE

	WWFE		GRAD	
FIT ENERGY	Mono	Stereo	Mono	Stereo
E1	0.5246	0.8274	0.4602	0.4890
E2	0.9914	0.8076	0.3936	0.2762
E3	0.6234	0.7696	0.9240	0.4720
E4	0.4866	0.2040	0.4002	0.7000
E5	0.2806	0.4386	0.9810	0.1846
E6	0.4748	...	0.6382	...
E1–E3 CP	0.8951	0.9700	0.7340	0.4808
Significance (σ).....	1.25	1.88	0.63	0.05

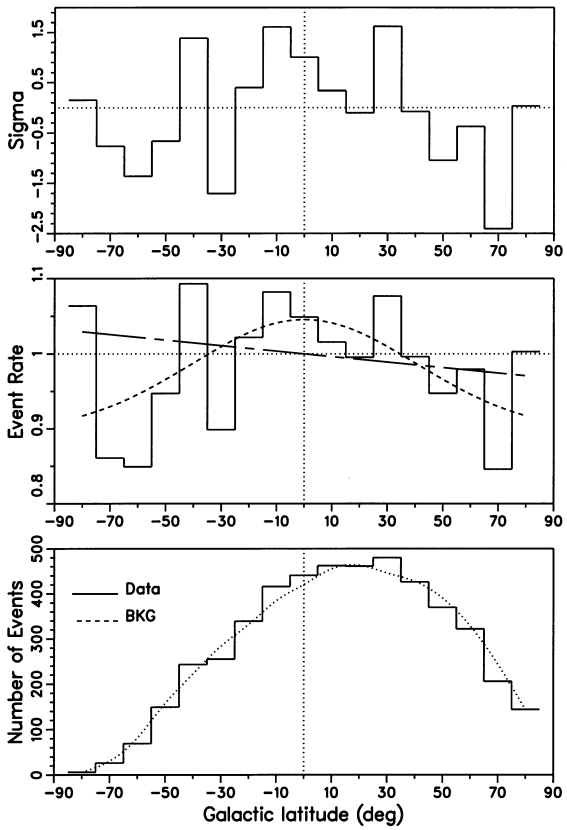

FIG. 11.—Monocular data and isotropic background distribution of the all-sky zone for 0.4–1.0 EeV. The bottom figure shows the histogram of the number of events as function of galactic latitude. The data (D_i) are represented by the histogram steps while the isotropic background (B_i) is the dotted line. The middle figure shows the event rate that is the ratio of number of events to background, D_i/B_i. The WWFE fit is shown by the dashed line and the gradient fit is shown by the dot-dashed line. The top figure shows the significance $(D_i - B_i)/S_i$.

Recently, the AGASA group reported a significant first harmonic at energy $10^{17.9}$–$10^{18.3}$ eV, with a chance probability of 0.005% (Hayashida et al. 1998). Considering the possible energy scale difference between the Fly's Eye and the AGASA, this range may well overlap with our range $10^{17.6}$–10^{18} eV. A detailed comparison of the two groups results is currently under study.

7. SUMMARY

1. We have reexamined both the monocular and stereo Fly's Eye data and looked for anisotropy related to galactic or supergalactic latitude. Two functional forms were studied. The first was the latitude gradient

$$I(b) = I_0(1 + f \times b)\,, \tag{17}$$

and the second was the plane enhancement factor

$$I(b) = I_0(1 - f + 1.437 \times f \times e^{-b^2})\,. \tag{18}$$

2. The isotropic background was calculated by scrambling the event arrival direction and trigger time. There were 5000 simulated data sets, each having the same number of events as the real data. The mean value of these 5000 sets was used to represent the distribution expected from isotropy. The standard deviation of these 5000 sets was used as the uncertainty in that distribution.

3. We find that the galactic plane enhancement factor f_E is nonzero at the 3.2 σ level for energies less than 3.2 EeV. The chance probability of such an anisotropy existing in these three energy bins is less than 0.06%. For energy 3.2 EeV, although a negative plane enhancement factor could be possible, the significance is less than 2 σ. The galactic latitude gradient is only significant in the energy range 0.4–1 EeV, where the galactic plane enhancement is strongest too. Overall, the galactic latitude gradient is not as significant as the galactic plane enhancement factor. One should bear in mind that the actual form of the anisotropy may be different from either the WWFE or GRAD functions.

4. No significant supergalactic latitude gradient or supergalactic plane enhancement factor has been found.

5. This analysis supports the view that the arrival directions of cosmic rays at energies less than 3.2 EeV are weakly correlated with the galactic plane. For energy greater than 3.2 EeV, no significant anisotropy is found.

We acknowledge the Department of the Army and the staff of Dugway Proving Ground for their cooperation and assistance. This work has been supported in part by the National Science Foundation (at Utah) and the US Department of Energy (at Illinois).

REFERENCES

Baltrusaitis, R. M., et al. 1985, Nucl. Instr. Meth., A240, 410
Bird, D. J., et al. 1993a, Proc. 23rd International Cosmic Ray Conference, Calgary, 2, 30
———. 1993b, Proc. 23rd International Cosmic Ray Conference, Calgary, 2, 38
———. 1993c, Proc. 23rd International Cosmic Ray Conference, Calgary, 2, 55
———. 1993d, Phys. Rev. Lett., 71, 3401
———. 1994, ApJ, 424, 491
Bhattacharjee, P., Hill, C. T., & Schramm, D. N. 1992, Phys. Rev. Lett., 69, 567
Bhattacharjee, P., & Sigl, G. 1995, Phys. Rev. D, 51, 4079
Cassiday, G. L. 1985, Ann. Rev. Nucl. Part. Sci., 33, 321
Chi, X., et al. 1993, J. Phys G, 19, 780
Eadie, W. T., et al. 1971, Statistical Methods in Experimental Physics (Amsterdam: North-Holland), 283
Fisher, R. A. 1958, Statistical Methods For Research Workers (13th ed.; New York: Hafner), 99
Gillerman, M. S., & Watson, A. A. 1993, Proc. 23rd ICRC (Calgary), 2, 47
Hayashida, N., et al. 1998, ICRR preprint
Huang, M. A. 1996, Ph.D thesis, Univ. Utah
Kewley, L. J., Clay, R. W., & Dawson, B. R. 1996, Astropart. Phys., 5, 69
Kronberg, P. P. 1994, Rep. Prog. Phys., 57, 325
Smith, A. G. K., & Clay, R. W. 1991, Proc. 22 ICRC (Dublin), 2, 129
Stanev, T., et al. 1995, Phys. Rev. Lett., 75, 3056
Waxman, E., Fisher, K. B., & Piran, T. 1997, ApJ, 483, 1
Wdowczyk, J., & Wolfendale, A. W. 1984, J. Phys. G, 10, 1453